Geophysical Research Letters

RESEARCH LETTER
10.1029/2024GL110206

Io's Near-Field Alfvén Wings and Local Electron Beams Inferred From Juno/Waves

A. H. Sulaiman[1], W. S. Kurth[2], J. E. P. Connerney[3,4], S. S. Elliott[1], G. B. Hospodarsky[2], N. S. Kruegler[1], R. L. Lysak[1], J. D. Menietti[2], J. R. Szalay[5], F. Allegrini[6,7], and S. J. Bolton[6]

[1]School of Physics and Astronomy, Minnesota Institute for Astrophysics, University of Minnesota, Minneapolis, MN, USA, [2]Department of Physics and Astronomy, University of Iowa, Iowa City, IA, USA, [3]Space Research Corporation, Annapolis, MD, USA, [4]NASA/Goddard Space Flight Center, Greenbelt, MD, USA, [5]Department of Astrophysical Sciences, Princeton University, Princeton, NJ, USA, [6]Southwest Research Institute, San Antonio, TX, USA, [7]Department of Physics and Astronomy, University of Texas at San Antonio, San Antonio, TX, USA

Key Points:

- Juno plasma wave observations are consistent with Alfvén wing crossings during close Io flybys
- Whistler-mode radiation indicate the presence of sub-keV electron beams operating just outside the Alfvén wing
- Electron densities are significantly elevated in Io's polar region

Supporting Information:

Supporting Information may be found in the online version of this article.

Correspondence to:

A. H. Sulaiman,
asulai@umn.edu

Citation:

Sulaiman, A. H., Kurth, W. S., Connerney, J. E. P., Elliott, S. S., Hospodarsky, G. B., Kruegler, N. S., et al. (2024). Io's near-field Alfvén wings and local electron beams inferred from Juno/Waves. *Geophysical Research Letters*, *51*, e2024GL110206. https://doi.org/10.1029/2024GL110206

Received 8 MAY 2024
Accepted 19 JUL 2024

Abstract Juno conducted two close Io flybys on 30 December 2023 and 03 February 2024, both at a minimum altitude of 1,500 km. Filamentary structures in the electric and magnetic field spectra indicate Juno crossed the Alfvén wing, the magnetic structure connecting Io to Jupiter's polar ionosphere. We show that the first pass took Juno diametrically through the northern Alfvén wing, while the second pass had Juno graze the southern Alfvén wing boundary, enabling extended measurements of the transition region between Io's vicinity and the Jovian magnetosphere. Of note, evidence of local electron beams is inferred from whistler-mode emissions. We demonstrate that their energies are sub-keV, are sourced from Io's ionosphere or local torus, and are part of a distributed current system connecting Io to Jupiter. Finally, upper hybrid resonances indicate electron densities are significantly elevated in Io's polar region (~28,000 cm^{-3}) compared to the local Io torus (~2,000 cm^{-3}).

Plain Language Summary Juno conducted two close Io flybys. Signatures in the electromagnetic field indicate that Juno sampled the region dominated by the electrodynamic interaction between Io and Jupiter. Powerful electric currents flow within this region that deliver energetic electrons into Jupiter's polar atmosphere, resulting in the Io auroral footprint. Juno also spent an extended period along the boundary of this region, providing an in situ view of the complexity of this region's structure. Local density measurements indicate significantly elevated densities in Io's poles.

1. Introduction

As the Juno spacecraft's perijove continues to migrate northward in the extended mission phase, it progressively crosses Jupiter's equator at smaller radial distances. This has permitted close and distant flybys of three of the innermost Galilean moons beginning with Ganymede (e.g., Clark et al., 2022; Duling et al., 2022; Hansen et al., 2022; Kurth et al., 2022), Europa (e.g., Kurth et al., 2023; Szalay, Allegrini, et al., 2024), and most recently two close flybys of Io. These took place on 30 December 2023 and 03 February 2024. On both occasions, Juno traversed magnetic field lines connecting Io to Jupiter's polar ionosphere. These magnetic structures protruding from Io, called the Alfvén wings, carry powerful field-aligned currents of the order of 1 MA (Acuña et al., 1981; Saur et al., 1999; Sulaiman et al., 2023). As a result, a rich set of observables are associated with these structures, not only in Io's neighborhood as reported during the Galileo era, but also from Juno's high-latitude crossing of flux tubes connected to Io's auroral footprint. Various facets of the electrodynamic interaction revealed by Juno, thus far, include electron and proton acceleration (Szalay et al., 2018, 2020a, 2020b; Szalay, Saur, et al., 2024), energetic particle dynamics (Clark et al., 2020, 2023; Paranicas et al., 2019, 2024), magnetic field fluctuations (Gershman et al., 2019; Janser et al., 2022; Sulaiman et al., 2023), and plasma waves of multiple scales (Sulaiman et al., 2020).

This letter provides an overview of the Juno plasma wave observations during the two close flybys of Io more than 20 years after Galileo's last flyby of the moon. We show that Juno crossed through and was magnetically connected to the Alfvén wing on both occasions, respectively, and highlight the similarities and differences between the two. The highly elliptical, polar orbits of Juno have enabled excellent spatial coverage of Io's Alfvén wings, providing multi-point measurements from the high-latitude (Jupiter-end) to the equatorial (Io-end) of the flux tube

across the mission. As a result, we anticipate in the near future continued progress toward a complete picture of the complex Io-Jupiter electrodynamic interaction.

2. Flyby Geometry

The Waves instrument (Kurth et al., 2017) consists of an electric field dipole antenna measuring one component of the wave electric field in the spacecraft's spin plane, effectively providing the capability of measuring two components of the wave electric field twice per spin of period 30 s. A search coil antenna mounted on the spacecraft's spin axis measures one component of the wave magnetic field independently of spin. We utilize Waves data from two receivers at a sampling rate of 50 kilosamples per second: the dual-channel Low-Frequency Receiver Low Band (LFR-Lo) which covers the frequency range of 50 Hz to 20 kHz simultaneously for both the E- and B-fields, the Low-Frequency Receiver High Band (LFR-Hi) and the High-Frequency Receiver Low Band (HFR-Hi), which cover the frequency ranges of 10 kHz–150 kHz and 100 kHz–3 MHz, respectively, for only the E-field. This frequency range is sufficient to capture plasma waves below and above the electron plasma and cyclotron frequencies, given the range of densities and magnetic field strengths in Io's vicinity. The Waves suite further provides the capability to distinguish between quasi-electrostatic, $\delta E(f) \gg c\delta B(f)$, and electromagnetic, $\delta E(f) \sim c\delta B(f)$, waves below 20 kHz with the caveat that not all six E- and B-field components are measured simultaneously.

The two close Io flybys occurred before Juno's 57th perijove on 30 December 2023 and before the 58th perijove on 03 February 2024. Figure 1 illustrates the geometry of the flybys in the Io-centered right-handed Io-Phi-Omega (IPhiO) coordinate system, where $+Z$ is aligned with Jupiter's spin axis (primary axis) and $+Y$ is in the direction of the component of the Io-Jupiter vector perpendicular to $+Z$ (secondary axis). The $+X$ direction completes the right-handed system and is aligned with the rigid corotation direction. Both flybys brought Juno to an altitude of 1,500 km at closest approach, with Io located in System-III west longitudes/centrifugal latitudes (Phipps & Bagenal, 2021) of 132°/+2.7° and 334°/–4.5°, respectively. During PJ57 (PJ58), Juno was north (south) of Io and in its leading (leading) hemisphere at closest approach. The flow streamlines in Figures 1a and 1c are constructed from a model developed for Io (Saur et al., 1999), also used to estimate the location of the Alfvén wing center at $Z = +1.8$ R_{Io} and -1.3 R_{Io}, respectively. Their inclusion is meant to provide qualitative context to the Waves observations.

Overlaid on each trajectory plot are the magnetic field spectral densities at 100 Hz measured along Juno's spin axis, which was approximately perpendicular to the background magnetic field for both flybys. The proton cyclotron frequency, f_{cH+}, was measured at ∼30 Hz and this is below the minimum frequency of 50 Hz measured by Waves. Thus, these are the powers of transverse high-frequency/small-scale fluctuations up to several times f_{cH+} but well below f_{ce}. During both flybys, there are sharp boundaries, within which the power changes over five orders of magnitude greater than the background in the vicinity of Io. In the next section, we will expand on our interpretation of these sudden changes as traversals of the Alfvén wing and its boundary. Geometrically, their locations are consistent with where we expect the Alfvén wings to be situated. For PJ57 (PJ58), the region of enhanced wave power in Io's northern (southern) hemisphere is in Io's sub-Jovian side, consistent with its location in Jupiter's northern (southern) centrifugal latitude where the magnetospheric field is tilted toward Jupiter.

3. Plasma Wave Observations and Interpretation

Figure 2 shows plasma wave and magnetic field observations during the two flybys. Figures 2a and 2e are time series of the three components of the background-subtracted magnetic field (Connerney et al., 2017) in the IPhiO coordinate system. Large (spatial) gradients in the magnetic field are indicative of strong currents. Figures 2b and 2c, 2f and 2g are the frequency-time electric field spectral densities, and Figures 2d and 2h the frequency-time magnetic field spectral densities, all measured by the Waves instrument. The electron cyclotron frequency is 56 and 50 kHz for PJ57 and PJ58, respectively, with the difference primarily attributed to the difference in magnetic latitudes. During both flybys, there was a sudden onset and subsequent cessation of intense broadband electric and magnetic field substructures up to a few times the proton cyclotron frequency (∼30 Hz). Such signatures are reminiscent of those reported from the Galileo/PWS measurements during Io Alfvén wing crossings (Chust et al., 2005). During PJ57, Juno traversed the predicted Alfvén wing cross-section almost diametrically, from the anti- to the sub-Jovian sides and from the leading to the trailing hemispheres. The enhancements in

10.1029/2024GL110206

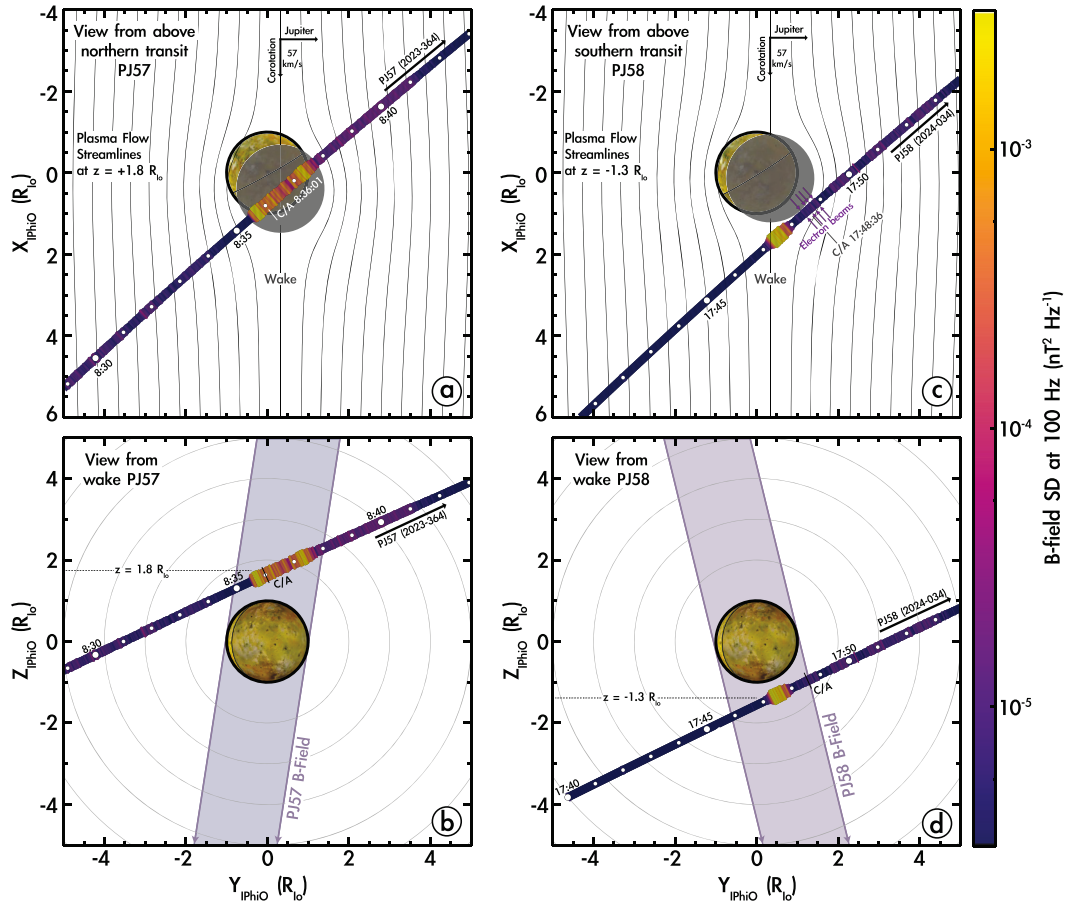

Figure 1. (left) *X-Y* and *Y-Z* projections of Juno's trajectory in the Io-Centered IPhiO coordinate system, as defined in text, during PJ57. (Right) Same during PJ58. These are normalized to the Io radius, R_{Io}, of 1,821 km. The magnetic field spectral density at 100 Hz is overlaid, as measured by the search-coil magnetometer which was oriented approximately perpendicular to the background magnetic field during both flybys. The gray disks in the *X-Y* plane represent the cross-sectional area of the modeled Alfvén wing at $Z = +1.8\ R_{Io}$ (PJ57) and $-1.3\ R_{Io}$ (PJ58) using an Alfvén Mach numbers of 0.4 and 0.2, respectively, which control the bend-back angle with respect to Io, and an ionospheric scale height 150 km, which sets the radius at R_{Io} + 150 km. More details on the modeled streamlines can be found in Saur et al. (1999) and Szalay, Saur, et al. (2024).

electric and magnetic field fluctuations, interpreted to mark the Alfvén wing boundary, appear contemporaneously with the inner edges of the magnetic field gradients. The interval was from 08:35:30 until 08:37:56.

We can estimate the field-aligned current direction, roughly along *Z*, from the sign of $\left(\frac{\partial B_Y}{\partial X} - \frac{\partial B_X}{\partial Y}\right)$. With decreasing *X* and increasing *Y*, we observe a decrease in both dB_x and dB_y during entry at ∼08:35, followed by their increase during exit at ∼08:38. Thus, we deduce that the field-aligned currents are flowing along the boundaries, into Io's northern hemisphere on its sub-Jovian side and away on its anti-Jovian side. This is consistent with the structure of the current system inferred from high-latitude observations when Juno traversed the ionospheric end of the Alfvén wing that maps to Io's auroral spot (Sulaiman et al., 2023).

Within the Alfvén wing, Chust et al. (2005) postulated that these extended-in-frequency substructures measured by Galileo are due to filamentation/fragmentation of Alfvén waves that are initialized at the scale of Io. This mechanism promotes the escape of the Alfvén waves from the torus boundary allowing them to reach the high-latitude regions where significant electron acceleration occurs. Acceleration is possible because when electron inertia is accounted for, Alfvén waves become dispersive and can develop large parallel electric fields. In the low plasma β regime (in Jupiter's high-latitude region), the Inertial Alfvén Wave propagates, and the parallel electric field becomes important on perpendicular scales of the electron inertial length (Lysak et al., 2021, 2023; Saur et al., 2018). Thus, concluding filamentation would necessitate the signatures within Alfvén wings be interpreted

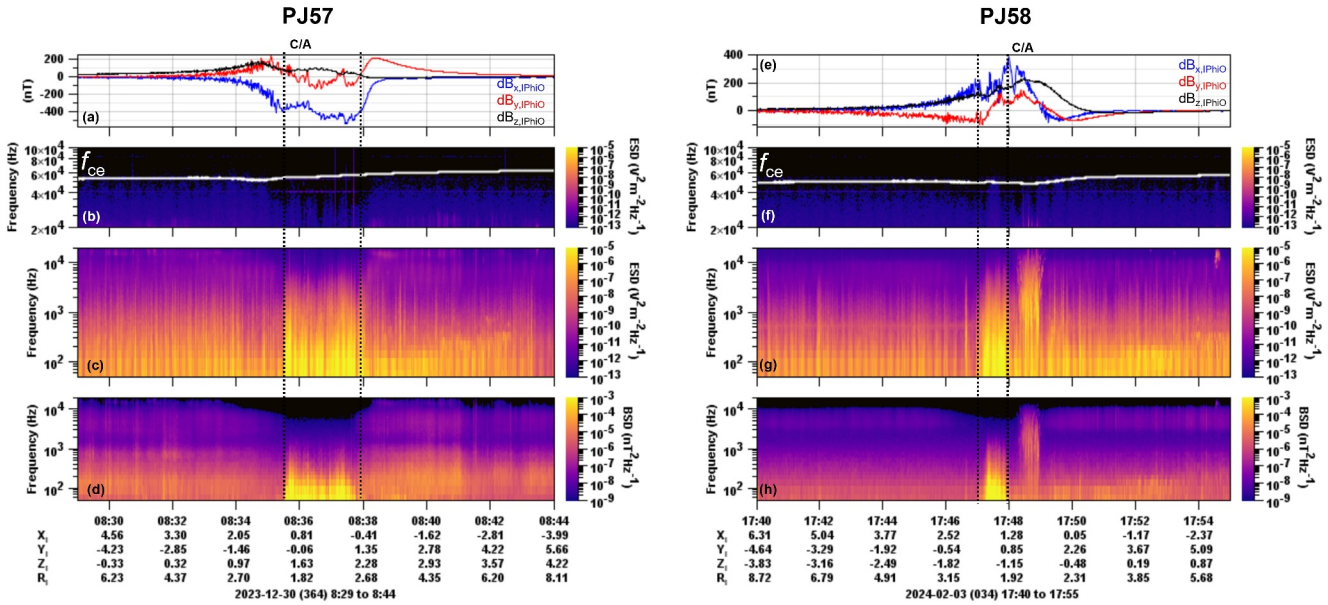

Figure 2. Plasma wave and magnetic field measurements during the PJ57 (left) and PJ58 (right) Io flybys. The top row are time series of the background-subtracted magnetic field, recorded by the magnetometer, and transformed into the IPhiO coordinate system. The second and third rows are frequency-time spectrograms of the electric field spectral densities with the electron cyclotron frequency, f_{ce}, overlaid; the fourth row are frequency-time spectrograms of the magnetic field spectral densities, all measured by the Waves instrument. The closest approach times (C/A) are indicated for both flybys. The intervals where intense electromagnetic substructures are present in the plasma wave data are delimited by dashed black lines. These are the same as the intervals as in Figure 1 and are interpreted as proxies for the Alfvén wing. Shorter intervals of these events can be found in Figure S1 in Supporting Information S1.

as spatial fluctuations. However, an ambiguity exists with single spacecraft time series measurements, whereby spatial versus temporal variability cannot be separated. Recent studies of Juno's sampling of high-latitude satellite flux tubes demonstrated that the measured Alfvénic Poynting and electron energy fluxes are coupled by an efficiency of ∼10%, that is, the fraction of electromagnetic energy that goes into accelerating electrons at the high latitudes (Sulaiman et al., 2023; Szalay et al., 2020c). This agrees with theoretically derived efficiencies (4%–10%) from energization of filamented waves obtained through a turbulent cascade (Hess et al., 2010, 2011), thus lending credence to the argument put forth by Chust et al. (2005).

The substructures are estimated to have a length scale of ∼100 km given the observation time of 2–5 s and a spacecraft speed of 30 km/s with respect to Io. Similar substructures in the electric and magnetic fields were observed during PJ58, albeit within a shorter timescale of ∼1 min (compared with ∼2.5 min during PJ57). The interval was from 17:47:00 until 17:47:59. Figure 1c illustrates that the spacecraft trajectory may have grazed the Alfvén wing boundary along a short chord of the cross section, as opposed to nearly along the diameter as in PJ57. Note that we have used the same ionospheric scale height to model the diameter of the Alfvén wing for both flybys, thus it is plausible that there may be a marked difference in scale heights between the two flybys. Indeed, Io was immersed father away from Jupiter's centrifugal equator during PJ58, where the magnetospheric plasma is densest, and the size of its southern Alfvén wing may respond to changes in pressure. However, simply inflating the Alfvén wing's diameter would cause the area to overlap with a longer segment of the trajectory to include times when the electromagnetic substructures were not observed. This event calls attention to how the Alfvén wing boundary is defined. Closer inspection of Figure 1c shows that the interval of electromagnetic substructures coincides with when Juno was magnetically mapped to the wake just downstream of the predicted Alfvén wing proper. The flow in the wake is unsteady and the embedded magnetospheric field, although past Io, is still deformed as it transitions back toward its "freestream" undeformed state further downstream (see Figure 4 in Neubauer (1980)). Another possibility could be that these "filamentary" signatures may instead be associated with reflected Alfvén waves returning from Jupiter and propagate just downstream of Io. However, we would expect the power in the magnetic field fluctuations to be markedly diminished in PJ58 compared to PJ57. Thus, we believe it is more likely that this region is an extension of the Main Alfvén Wing just downstream of Io.

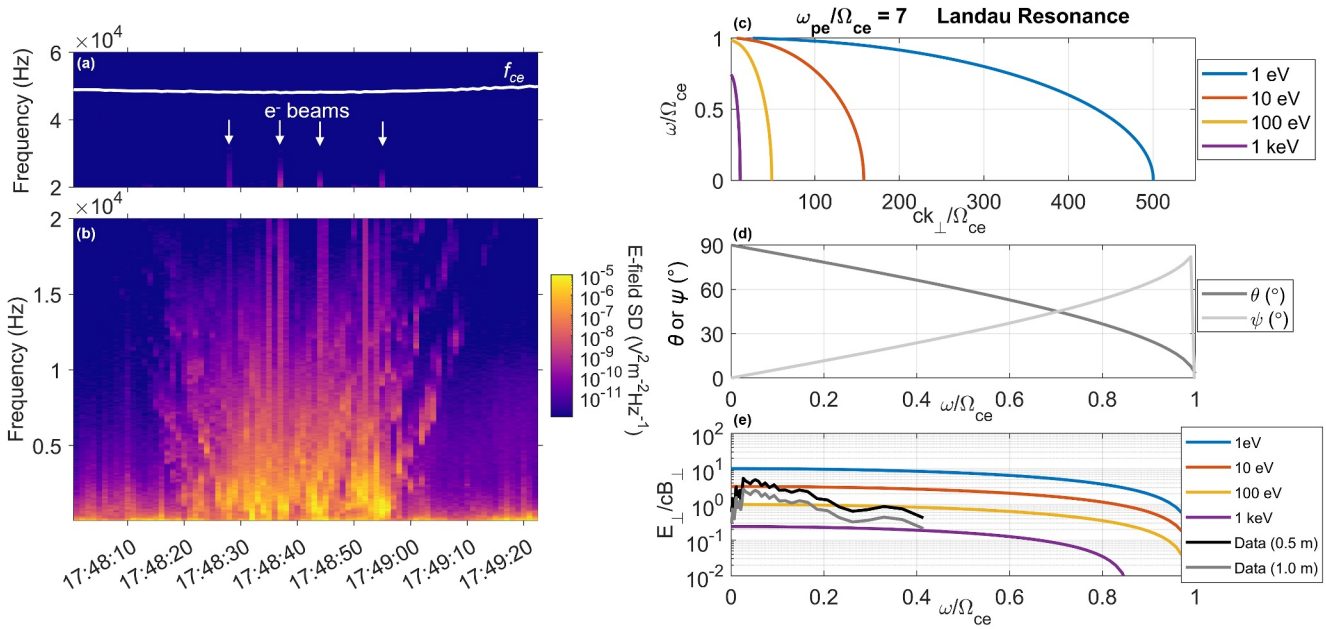

Figure 3. (a and b) Frequency-time spectrograms (from two channels) of the electric field spectral density during the PJ58 closest approach to Io. The electron cyclotron frequency, f_{ce}, is overlaid as a white solid line. Instances where electron beams are inferred to be present are indicated by white arrows. (c) Dispersion relation analysis of the whistler mode using the cold plasma approximation in the electron limit and invoking the Landau resonance condition for $f_{pe}/f_{ce} = 7$. Here, $\omega = 2\pi f$, $\Omega_{ce} = 2\pi f_{ce}$, and $\omega_{pe} = 2\pi f_{pe}$. (d) Theoretical wave normal, θ, and group velocity, ψ, angles with respect to the background magnetic field and along the resonance cone as a function of normalized frequency. (e) Theoretical and measured $E_\perp/cB_\perp$ ratios as a function of normalized frequency for a range of electron energies. The measured $E_\perp/cB_\perp$ is computed based on a realistic antenna effective length of 0.5 m. An effective length of 1.0 m is also added and its $E_\perp/cB_\perp$ may be taken as a lower limit.

Beyond this short interval, the plasma wave measurements indicate evidence of electron beams around closest approach, in the time interval 17:48:20–17:48:56. The locations are highlighted in Figure 1c. Figures 3a and 3b show the electric field spectral density from two channels centered around closest approach during the PJ58 Io flyby. The lowest channel (Figure 3b) shows clear dispersive structures in frequency-time well below the electron cyclotron frequency, f_{ce}, which is ~50 kHz (Figure 3a). These V-shaped structures are characteristic of whistler-mode auroral hiss, sometimes called "saucers," and are generated via a beam-plasma instability at the Landau resonance (Farrell et al., 1988; Maggs, 1989), where the parallel phase speed of the wave approximately matches the electron beam speed, $\omega/k_\parallel \approx v_{beam}$. Here, wave growth is fueled by the free energy from the unstable electron velocity anisotropy. For this reason, they are commonly observed on magnetic field lines carrying electron beams/field-aligned currents, provided the frequency is below both f_{ce} and f_{pe} (Gurnett et al., 2011; Kopf et al., 2010; Sulaiman et al., 2018; Xin et al., 2006).

In Figures 3c–3e, we employ the cold plasma dispersion relation to determine what electron energies can account for the observed frequencies in the whistler mode. Using the equations (e.g., Temerin & Lysak, 1984)

$$Sn_\perp^4 - \left[S^2 - D^2 + SP - n_\parallel^2 (S+P)\right] n_\perp^2 + P\left[\left(n_\parallel^2 - S\right)^2 - D^2\right] = 0 \quad (1)$$

$$S = 1 - \frac{f_{pe}^2}{f^2 - f_{ce}^2} \quad (2)$$

$$D = \frac{-f_{ce} f_{pe}^2}{f\left(f^2 - f_{ce}^2\right)} \quad (3)$$

$$P = 1 - \frac{f_{pe}^2}{f^2} \quad (4)$$

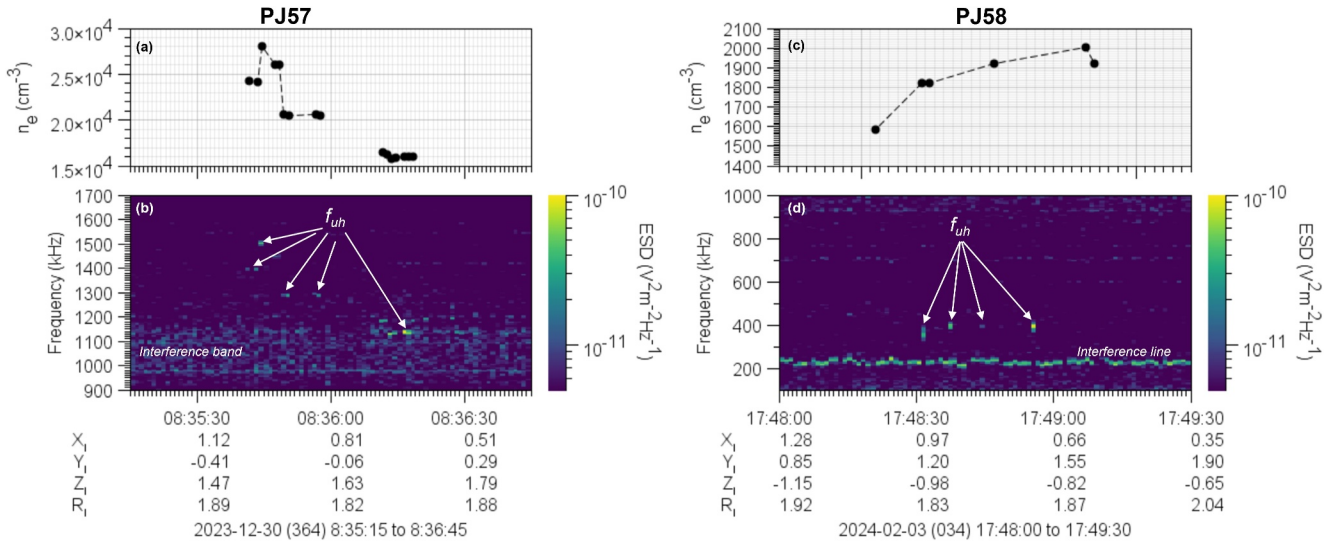

Figure 4. (top) Inferred electron densities from (bottom) upper hybrid resonances during (a and b) PJ57 and (c and d) PJ58 close Io flybys.

$$\tan^2\theta\,(n\to\infty) = -\frac{P}{S} \tag{5a}$$

$$\tan^2\psi\,(n\to\infty) = -\frac{S}{P} \tag{5b}$$

where the index of refraction $n_{\perp,\parallel} = ck_{\perp,\parallel}/\omega$. S, P, and D are elements of the dielectric tensor from the cold plasma dispersion relation as defined in Stix (1992). These are each a function of f_{ce} and f_{pe} and, in turn, the local magnetic field strength and electron density (see Figure 4). To solve Equation 1, we use the measured $f_{pe}/f_{ce} = 7$ and invoke the Landau resonance condition by setting $n_\parallel = c/v_{beam}$ for electron energies of 1 eV, 10 eV, 100 eV, and 1 keV. Figure 3c shows that real frequencies exist below f_{ce} and the dispersion is in agreement with propagation along the resonance cone. Figure 3d shows the wave normal angle, θ, and the group velocity (same as Poynting vector) angle, ψ, with respect to the background magnetic field. Along the resonance cone ($n \to \infty$), these are complementary angles, that is, $\theta + \psi = 90°$. The Waves instrument will detect a wave when the instrument sensors intercept the group velocity vector, since this is the direction of the flow of electromagnetic energy. Note that along the resonance cone, the waves are quasi-electrostatic (as opposed to purely electrostatic), thus can still carry Poynting fluxes. The angle, ψ, increases monotonically with frequency up to f_{ce}. In other words, low frequencies propagate parallel to the magnetic field, while higher frequencies monotonically develop a larger perpendicular component. Thus, the whistler mode propagating at a continuum of frequencies will exhibit a V-shaped feature in frequency-time as higher frequencies are detected earlier and later. The time when the lowest (parallel-propagating) frequency of the V-shaped emission is measured, that is, the vertex, can therefore be interpreted as the source magnetic field line along which the electron beams are co-located. In Figure 3b, we identify four distinct vertices that are irregularly spaced, thereby ruling out spin modulation. The times of these vertices are also when large amplitude waves, called electrostatic solitary structures (ESWs), are present and have been shown to have strong modulations with electron beams (Ergun et al., 1998). These are manifested as broadband-in-frequency signatures that extend up to the next frequency channel in Figure 3a.

Figure 3e relates the observed whistler-mode emissions to electron energies by comparing the theoretically computed with the measured E/cB ratios. Since the Waves instrument does not measure all six components of the E- and B- fields simultaneously, we restrict the comparison to $E_\perp$ and $B_\perp$ that is enabled by the spacecraft attitude. We find the measured $E_\perp/cB_\perp$ to agree with the theoretical counterpart when electron energies of 10 s of eV are chosen. These are significantly lower than the order keV populations that dominate in the Main Alfvén Wing (Sulaiman et al., 2020; Szalay et al., 2020a). The absence of the "filamentary" signatures and the association of the quasi-electrostatic whistler-mode emissions with intermediate electron energies lead us to conclude that this interval was outside the Main Alfvén Wing. That said, the gradients in the magnetic field indicate that the currents

are flowing toward Io during this interval, thus the source of the electron beams is Io's ionosphere or local torus. These currents are measured after sharp gradients at the 17:47:59 boundary that line up with the sudden cessation of the "filamentary" wave power (second dashed line in Figures 2e–2h). It therefore appears that there are currents and associated electron beams operating just outside the Alfvén wing, and although distinct, need not be entirely disconnected from the current system. This source of electron beams is likely a result of an extended interaction with the local torus around the Alfvén wing, where the flow and embedded magnetic field are perturbed but to a lesser extent and demand a lower $\mathbf{J} \times \mathbf{B}$ force to reaccelerate the flow. Observing this phenomenon during PJ58 can be explained by a trajectory effect, where Juno crossed the Alfvén wing tangentially thus spending more time in the boundary and surrounding regions, compared to the diametric traversal during PJ57. The Transhemispheric Electron Beam is ruled out since these are also of order keV and expected to be decoupled from the Alfvén wing in the northern hemisphere when Io is at a large southern centrifugal latitude (Bonfond et al., 2008).

Finally, we report on the observed electron densities in Io's vicinity. Figure 4 shows high-resolution plasma wave spectra from the highest frequency channel. Intermittent enhancements in Figures 4b and 4d are interpreted as resonances occurring at the upper hybrid frequency from which the local electron plasma frequency, and thus the electron density, can be derived as $f_{uh}{}^2 = f_{ce}{}^2 + f_{pe}{}^2$. During PJ57, signatures are present when Juno was within the northern Alfvén wing and the measured electron densities were elevated at $1.5–2.8 \times 10^4$ cm^{-3}. These numbers are similar to those reported by Galileo/PWS directly over the poles of Io (Gurnett et al., 2001). That said, the upper hybrid resonance (UHR) measured by Galileo/PWS was a continuous emission line, rather than intermittent as reported here. This can be explained by a difference in instrument performance. Close inspection of the Galileo data (Figure 1 in Gurnett et al. (1996)) will show that the UHR emission, although continuous, has intermittent peaks in the intensity. The high-frequency band in Juno/Waves has higher noise and lower sensitivity. Therefore, we are only detecting the UHR emission when the intensity is above a threshold (see Figure 27 in Kurth et al. (2017)). The electron densities measured during PJ58 were, by contrast, in the range 1,500–2,000 cm^{-3} and consistent with Io torus measurements reported from Galileo/PWS (Gurnett et al., 1996). These were measured in the interval where the local electron beams were observed, thus supporting our conclusion that the beams are operating outside the Alfvén wing.

4. Conclusions

This letter presents an overview of the Juno plasma wave observations during the two close Io flybys. During the first pass (before PJ57), Juno crossed the northern Alfvén wing nearly diametrically and its sharp boundaries were identified from sudden onset and subsequent cessation of "filamentary" electromagnetic emissions that are extended in frequency up to a few times the proton cyclotron frequency. The boundaries coincided with the inner edges of magnetic field gradients that are indicative of currents flowing into Io's northern hemisphere on its sub-Jovian side and away on its anti-Jovian side. Upper hybrid resonances measured during the northern Alfvén Wing crossing indicate electron densities are elevated in Io's polar region.

During the second pass (before PJ58), Juno grazed the Alfvén wing along a direction tangential to the boundary. A much shorter interval of the "filamentary" electromagnetic emissions just downstream of Io indicate that Juno was magnetically connected to the immediate wake, where the magnetic field is still deformed. Upon exit, and at closest approach, quasi-electrostatic whistler-mode emissions were observed with a dispersion that is fully consistent with a beam-plasma instability. The measured E/cB ratio can be explained by electron energies of 10 s of eV, markedly lower than the order keV populations that dominate in the Alfvén wing proper. We conclude that Juno's extended time along the boundary enabled sampling of the transition region between the Alfvén wing proper and the Jovian magnetosphere proper, that is characterized by flow and field perturbations that are appreciable but weaker than that of the Alfvén wing. Magnetic field gradients indicating distributed currents and electron densities consistent with those of the local Io torus support this interpretation.

Finally, electron density measurements were made possible through the detection of upper hybrid resonances. These indicated significantly elevated densities over Io's pole (~28,000 cm^{-3}) and typical densities in Io's local torus (~2,000 cm^{-3}).

Data Availability Statement

The calibrated Waves (JNO-E/J/SS-WAV-3-CDR-SRVFULL-V2.0) and MAG (JNO-J-3-FGM-CAL-V1.0) data used are from the Planetary Plasma Interactions Node in the Planetary Data System (Connerney, 2022; Kurth & Piker, 2022).

Acknowledgments
The research at the University of Minnesota is supported by NASA through contract S99022AKP with the Southwest Research Institute. The research at the University of Iowa is supported by NASA through Contract 699041X with the Southwest Research Institute. JDM acknowledges support from NASA Grant 80NSSC19K1262. WSK acknowledges the use of the Space Physics Data Repository at the University of Iowa supported by the Roy J. Carver Charitable Trust.

References

Acuña, M. H., Neubauer, F. M., & Ness, N. F. (1981). Standing Alfvén wave current system at Io: Voyager 1 observations. *Journal of Geophysical Research*, *86*(A10), 8513–8521. https://doi.org/10.1029/JA086iA10p08513

Bonfond, B., Grodent, D., Gérard, J.-C., Radioti, A., Saur, J., & Jacobsen, S. (2008). UV Io footprint leading spot: A key feature for understanding the UV Io footprint multiplicity? *Geophysical Research Letters*, *35*(5), 2007GL032418. https://doi.org/10.1029/2007GL032418

Chust, T., Roux, A., Kurth, W. S., Gurnett, D. A., Kivelson, M. G., & Khurana, K. K. (2005). Are Io's Alfvén wings filamented? Galileo observations. *Planetary and Space Science*, *53*(4), 395–412. https://doi.org/10.1016/j.pss.2004.09.021

Clark, G., Kollmann, P., Mauk, B. H., Paranicas, C., Haggerty, D., Rymer, A., et al. (2022). Energetic charged particle observations during Juno's close flyby of Ganymede. *Geophysical Research Letters*, *49*(23), e2022GL098572. https://doi.org/10.1029/2022GL098572

Clark, G., Mauk, B. H., Kollmann, P., Szalay, J. R., Sulaiman, A. H., Gershman, D. J., et al. (2020). Energetic proton acceleration associated with Io's footprint tail. *Geophysical Research Letters*, *47*(24). https://doi.org/10.1029/2020GL090839

Clark, G., Szalay, J. R., Sulaiman, A. H., Saur, J., Kollmann, P., Mauk, B. H., et al. (2023). Energetic proton acceleration by EMIC waves in Io's footprint tail. *Frontiers in Astronomy and Space Sciences*, *10*. https://doi.org/10.3389/fspas.2023.1016345

Connerney, J. E. P. (2022). Juno MAG CALIBRATED DATA J V1.0, JNO-J-3-FGM-CAL-V1.0 [Dataset]. *NASA Planetary Data System*. https://doi.org/10.17189/1519711

Connerney, J. E. P., Benn, M., Bjarno, J. B., Denver, T., Espley, J., Jorgensen, J. L., et al. (2017). The Juno magnetic field investigation. *Space Science Reviews*, *213*(1), 39–138. https://doi.org/10.1007/s11214-017-0334-z

Duling, S., Saur, J., Clark, G., Allegrini, F., Greathouse, T., Gladstone, R., et al. (2022). Ganymede MHD model: Magnetospheric context for Juno's PJ34 flyby. *Geophysical Research Letters*, *49*(24), e2022GL101688. https://doi.org/10.1029/2022GL101688

Ergun, R. E., Carlson, C. W., McFadden, J. P., Mozer, F. S., Delory, G. T., Peria, W., et al. (1998). FAST satellite observations of large-amplitude solitary structures. *Geophysical Research Letters*, *25*(12), 2041–2044. https://doi.org/10.1029/98GL00636

Farrell, W. M., Gurnett, D. A., Banks, P. M., Bush, R. I., & Raitt, W. J. (1988). An analysis of whistler mode radiation from the Spacelab 2 electron beam. *Journal of Geophysical Research*, *93*(A1), 153–161. https://doi.org/10.1029/JA093iA01p00153

Gershman, D. J., Connerney, J. E. P., Kotsiaros, S., DiBraccio, G. A., Martos, Y. M., Viñas, A. F., et al. (2019). Alfvénic fluctuations associated with Jupiter's auroral emissions. *Geophysical Research Letters*, *46*(13), 7157–7165. https://doi.org/10.1029/2019GL082951

Gurnett, D. A., Averkamp, T. F., Schippers, P., Persoon, A. M., Hospodarsky, G. B., Leisner, J. S., et al. (2011). Auroral hiss, electron beams and standing Alfvén wave currents near Saturn's Moon Enceladus. *Geophysical Research Letters*, *38*(6). https://doi.org/10.1029/2011GL046854

Gurnett, D. A., Kurth, W. S., Roux, A., Bolton, S. J., & Kennel, C. F. (1996). Galileo plasma wave observations in the Io plasma torus and near Io. *Science*, *274*(5286), 391–392. https://doi.org/10.1126/science.274.5286.391

Gurnett, D. A., Persoon, A. M., Kurth, W. S., Roux, A., & Bolton, S. J. (2001). Electron densities near Io from Galileo plasma wave observations. *Journal of Geophysical Research*, *106*(A11), 26225–26232. https://doi.org/10.1029/2000JA002509

Hansen, C. J., Bolton, S., Sulaiman, A. H., Duling, S., Bagenal, F., Brennan, M., et al. (2022). Juno's close encounter with Ganymede—An overview. *Geophysical Research Letters*, *49*(23), e2022GL099285. https://doi.org/10.1029/2022GL099285

Hess, S. L. G., Delamere, P., Dols, V., Bonfond, B., & Swift, D. (2010). Power transmission and particle acceleration along the Io flux tube. *Journal of Geophysical Research*, *115*(A6). https://doi.org/10.1029/2009JA014928

Hess, S. L. G., Delamere, P. A., Dols, V., & Ray, L. C. (2011). Comparative study of the power transferred from satellite-magnetosphere interactions to auroral emissions. *Journal of Geophysical Research*, *116*(A1). https://doi.org/10.1029/2010JA015807

Janser, S., Saur, J., Clark, G., Sulaiman, A. H., & Szalay, J. R. (2022). Properties of turbulent Alfvénic fluctuations and wave-particle interaction associated with Io's footprint tail. *Journal of Geophysical Research: Space Physics*, *127*(12). https://doi.org/10.1029/2022JA030675

Kopf, A. J., Gurnett, D. A., Menietti, J. D., Schippers, P., Arridge, C. S., Hospodarsky, G. B., et al. (2010). Electron beams as the source of whistler-mode auroral hiss at Saturn. *Geophysical Research Letters*, *37*(9), 2010GL042980. https://doi.org/10.1029/2010GL042980

Kurth, W. S., Hospodarsky, G. B., Kirchner, D. L., Mokrzycki, B. T., Averkamp, T. F., Robison, W. T., et al. (2017). The Juno waves investigation. *Space Science Reviews*, *213*(1), 347–392. https://doi.org/10.1007/s11214-017-0396-y

Kurth, W. S., & Piker, C. W. (2022). JUNO E/J/S/SS WAVES CALIBRATED SURVEY FULL RESOLUTION V2.0, JNO-E/J/SS-WAV-3-CDR-SRVFULL-V2.0 [Dataset]. *NASA Planetary Data System*. https://doi.org/10.17189/1520498

Kurth, W. S., Sulaiman, A. H., Hospodarsky, G. B., Menietti, J. D., Mauk, B. H., Clark, G., et al. (2022). Juno plasma wave observations at Ganymede. *Geophysical Research Letters*, *49*(23), e2022GL098591. https://doi.org/10.1029/2022GL098591

Kurth, W. S., Wilkinson, D. R., Hospodarsky, G. B., Santolík, O., Averkamp, T. F., Sulaiman, A. H., et al. (2023). Juno plasma wave observations at Europa. *Geophysical Research Letters*, *50*(24), e2023GL105775. https://doi.org/10.1029/2023GL105775

Lysak, R. L., Song, Y., Elliott, S., Kurth, W., Sulaiman, A. H., & Gershman, D. (2021). The Jovian ionospheric Alfvén resonator and auroral particle acceleration. *Journal of Geophysical Research: Space Physics*, *126*(12). https://doi.org/10.1029/2021JA029886

Lysak, R. L., Sulaiman, A. H., Bagenal, F., & Crary, F. (2023). A numerical model for the interaction of Io-generated Alfvén waves with Jupiter's magnetosphere and ionosphere. *Journal of Geophysical Research: Space Physics*, *128*(4), e2022JA031180. https://doi.org/10.1029/2022JA031180

Maggs, J. E. (1989). Nonlinear evolution of the auroral electron beam. *Journal of Geophysical Research*, *94*(A4), 3631–3651. https://doi.org/10.1029/JA094iA04p03631

Neubauer, F. M. (1980). Nonlinear standing Alfvén wave current system at Io: Theory. *Journal of Geophysical Research*, *85*(A3), 1171–1178. https://doi.org/10.1029/JA085iA03p01171

Paranicas, C., Mauk, B. H., Clark, G., Kollmann, P., Nénon, Q., Ebert, R. W., et al. (2024). Energetic charged particle measurements during Juno's two close Io flybys. *Geophysical Research Letters*, *51*(13), e2024GL109495. https://doi.org/10.1029/2024GL109495

Paranicas, C., Mauk, B. H., Haggerty, D. K., Clark, G., Kollmann, P., Rymer, A. M., et al. (2019). Io's effect on energetic charged particles as seen in Juno data. *Geophysical Research Letters*, *46*(23), 13615–13620. https://doi.org/10.1029/2019GL085393

Phipps, P., & Bagenal, F. (2021). Centrifugal equator in Jupiter's plasma sheet. *Journal of Geophysical Research: Space Physics*, *126*(1), e2020JA028713. https://doi.org/10.1029/2020JA028713

Saur, J., Janser, S., Schreiner, A., Clark, G., Mauk, B. H., Kollmann, P., et al. (2018). Wave-particle interaction of Alfvén waves in Jupiter's magnetosphere: Auroral and magnetospheric particle acceleration. *Journal of Geophysical Research: Space Physics*, *123*(11), 9560–9573. https://doi.org/10.1029/2018JA025948

Saur, J., Neubauer, F. M., Strobel, D. F., & Summers, M. E. (1999). Three-dimensional plasma simulation of Io's interaction with the Io plasma torus: Asymmetric plasma flow. *Journal of Geophysical Research*, *104*(A11), 25105–25126. https://doi.org/10.1029/1999JA900304

Stix, T. H. (1992). *Waves in plasmas*. American Institute of Physics.

Sulaiman, A. H., Hospodarsky, G. B., Elliott, S. S., Kurth, W. S., Gurnett, D. A., Imai, M., et al. (2020). Wave-particle interactions associated with Io's auroral footprint: Evidence of Alfvén, ion cyclotron, and whistler modes. *Geophysical Research Letters*, *47*(22). https://doi.org/10.1029/2020GL088432

Sulaiman, A. H., Kurth, W. S., Hospodarsky, G. B., Averkamp, T. F., Ye, S., Menietti, J. D., et al. (2018). Enceladus auroral hiss emissions during Cassini's Grand finale. *Geophysical Research Letters*, *45*(15), 7347–7353. https://doi.org/10.1029/2018GL078130

Sulaiman, A. H., Szalay, J. R., Clark, G., Allegrini, F., Bagenal, F., Brennan, M. J., et al. (2023). Poynting fluxes, field-aligned current densities, and the efficiency of the Io-Jupiter electrodynamic interaction. *Geophysical Research Letters*, *50*(10), e2023GL103456. https://doi.org/10.1029/2023GL103456

Szalay, J. R., Allegrini, F., Bagenal, F., Bolton, S. J., Bonfond, B., Clark, G., et al. (2020a). A new framework to explain changes in Io's footprint tail electron fluxes. *Geophysical Research Letters*, *47*(18). https://doi.org/10.1029/2020GL089267

Szalay, J. R., Allegrini, F., Bagenal, F., Bolton, S. J., Bonfond, B., Clark, G., et al. (2020c). Alfvénic acceleration sustains Ganymede's footprint tail aurora. *Geophysical Research Letters*, *47*(3). https://doi.org/10.1029/2019GL086527

Szalay, J. R., Allegrini, F., Ebert, R. W., Bagenal, F., Bolton, S. J., Fatemi, S., et al. (2024). Oxygen production from dissociation of Europa's water-ice surface. *Nature Astronomy*, *8*(5), 1–10. https://doi.org/10.1038/s41550-024-02206-x

Szalay, J. R., Bagenal, F., Allegrini, F., Bonfond, B., Clark, G., Connerney, J. E. P., et al. (2020b). Proton acceleration by Io's Alfvénic interaction. *Journal of Geophysical Research: Space Physics*, *125*(1). https://doi.org/10.1029/2019JA027314

Szalay, J. R., Bonfond, B., Allegrini, F., Bagenal, F., Bolton, S., Clark, G., et al. (2018). In situ observations connected to the Io footprint tail aurora. *Journal of Geophysical Research: Planets*, *123*(11), 3061–3077. https://doi.org/10.1029/2018JE005752

Szalay, J. R., Saur, J., Allegrini, F., Ebert, R. W., Valek, P. W., Clark, G., et al. (2024). Ion precipitation to Io's poles driven by a strong sub-Alfvénic interaction. *Geophysical Research Letters*, *51*, e2024GL110205. https://doi.org/10.1029/2024GL110205

Temerin, M., & Lysak, R. L. (1984). Electromagnetic ion cyclotron mode (ELF) waves generated by auroral electron precipitation. *Journal of Geophysical Research*, *89*(A5), 2849–2859. https://doi.org/10.1029/JA089iA05p02849

Xin, L., Gurnett, D. A., & Kivelson, M. G. (2006). Whistler mode auroral hiss emissions observed near Jupiter's Moon Io. *Journal of Geophysical Research*, *111*(A4), 2005JA011411. https://doi.org/10.1029/2005JA011411